Journal of Materials Chemistry B

ROYAL SOCIETY OF CHEMISTRY

PAPER

Published on 13 July 2026
Licensed under CC-BY-NC 4.0

Check for updates

Cite this: *J. Mater. Chem. B*, 2026, **14**, 9676

# Engineering a scaffold to control cell fates of stem cells for cartilage tissue engineering

Bowu Peng,[ab] Huajian Chen,[a] Tianjiao Zeng,[a] Mingxin Zhang,[ab] Toru Yoshitomi,[a] Naoki Kawazoe,[a] Yingnan Yang[c] and Guoping Chen *[ab]

Received 22nd April 2026,
Accepted 12th July 2026

DOI: 10.1039/d6tb00939e

rsc.li/materials-b

Precise spatial and temporal control of the fates of mesenchymal stromal cells (MSCs) through dynamic microenvironmental cues is essential for MSC-based tissue engineering. Artificial niches that recapitulate the spatiotemporal regulation of cell fates have been regarded as ideal platforms. Here, we engineered an artificial niche scaffold by integrating growth and chondrogenic induction factors that exerted staged effects on MSCs to direct different phases of cartilage regeneration. The scaffold was prepared by immobilizing heparin-binding epidermal growth factor-like growth factor and matrix metalloproteinase-2-cleavable peptide-tethered kartogenin-loaded liposomes within a gelatin/heparin/γ-PGA scaffold. The immobilized growth factor initially promoted MSC proliferation. The upregulation of proliferation-associated signaling served as an autonomous trigger for the subsequent release of kartogenin, thereby inducing MSC chondrogenesis. The results indicated that this spatiotemporally programmed system was able to regulate cellular fates in a spatiotemporal manner and promote cartilage regeneration.

## 1. Introduction

Cartilage injury and related diseases are considered major causes of physical disability worldwide, imposing a substantial socioeconomic burden on modern society. As a connective tissue with an avascular structure and no innervation, cartilage has limited self-healing capacity because of its unique properties.[1] Traditional strategies for cartilage defect treatment are limited and do not restore the intrinsic regenerative capacity of cartilage.[2,3] Therefore, developing new treatments that enable effective intrinsic repair of cartilage diseases is essential. In recent years, mesenchymal stromal cell (MSC)-based tissue engineering has attracted considerable attention as a promising strategy for cartilage regeneration, owing to the multipotent properties of MSCs.[3–8] This process generally proceeds in a stepwise manner, encompassing sequential proliferation and differentiation. Hence, precise control of MSC fate is pivotal for therapeutic outcomes.[9–11]

In the body, stem cells reside in instructive, tissue-specific microenvironments, or niches, that modulate stem cell fate.[12,13] Niches are dynamic and complex, autonomously regulating cellular behaviors during tissue repair.[14,15] When injuries occur, stem cells migrate to lesion sites, where they rapidly proliferate and subsequently differentiate into specific phenotypes to facilitate tissue regeneration. Inspired by the functions of natural niches, artificial niches that recapitulate instructive signals for tissue repair have attracted considerable attention in recent years.[10,16–20] However, the precise design of artificial niches to achieve their sequential functions during tissue repair remains a major challenge, the crux of which lies in identifying a trigger or signal that induces the subsequent differentiation process following cell proliferation.[11,21–24]

The extracellular matrix (ECM), as a predominant component of the niche and a reservoir of growth factors (GFs), plays important roles in providing anchoring sites, structural support, and GFs for the regulation of cellular fates.[14,25] During the tissue repair process, ECM remodeling occurs throughout the entire process, degrading the matrix to create space and release associated GFs that facilitate cell migration, proliferation, and differentiation, thereby maintaining tissue homeostasis.[26,27] Matrix metalloproteinases (MMPs) are endopeptidases that contribute to growth, development, wound healing, and pathogenesis through ECM remodeling. As major mediators of ECM remodeling, MMPs show promising potential as targets for recapitulating the precise manipulation of cell fates in artificial niches for tissue regeneration.[28,29] Among the various MMPs, MMP-2 has been identified as the most highly expressed during the normal proliferative behavior of stem cells.[30,31] Therefore, it may serve as a potential signaling cue to initiate the subsequent differentiation process and thereby promote tissue repair.

[a] *Research Center for Macromolecules and Biomaterials, National Institute for Materials Science, Ibaraki, 305-0044, Japan. E-mail: Guoping.CHEN@nims.go.jp*
[b] *Graduate School of Science and Technology, University of Tsukuba, Ibaraki, 305-8577, Japan*
[c] *Graduate School of Life and Environmental Science, University of Tsukuba, Ibaraki, 305-8572, Japan*


This journal is © The Royal Society of Chemistry 2026

Kartogenin (KGN), a small lipophilic molecule and chondrogenic induction factor, has been widely used in cartilage regeneration.[32] Liposomes, as nanoparticle-based delivery systems, have demonstrated a strong capacity for loading both hydrophilic and lipophilic drugs. Generally, hydrophilic drugs are encapsulated within the inner aqueous core, whereas lipophilic compounds are incorporated into the lipid bilayer of liposomes.[33] However, the incorporation of lipophilic compounds into the bilayer can destabilize the liposomal structure and cause rapid drug release, whereas drugs encapsulated within the aqueous core exhibit greater stability.[34,35] Cyclodextrins (CDs) are well-known for their ability to increase the solubility, dissolution rate, and bioavailability of loaded drugs.[36,37] In particular, CDs can form inclusion complexes with lipophilic compounds, thereby enhancing their solubility and bioavailability. Based on these properties, drug-in-CD-in-liposome systems have been widely used in drug delivery to achieve the stable encapsulation of lipophilic drugs.[36,37]

In this study, we designed and prepared an artificial niche scaffold that used endogenous MMP-2 as a trigger to release a chondrogenic induction factor, thereby promoting subsequent differentiation following cell proliferation and enabling investigation of the sequential proliferation and differentiation of MSCs during cartilage regeneration (Fig. 1). In our previous work,[38] we designed a heparin-functionalized scaffold with immobilized heparin-binding epidermal growth factor-like growth factor (HB-EGF) to mimic the regulatory functions of the ECM in controlling MSC fate. The results showed that immobilized HB-EGF enhanced MSC proliferation without inducing spontaneous differentiation. Subsequently, the supplement of differentiation factors is required to induce the chondrogenic differentiation of MSCs following proliferation. Based on this concept, KGN was first combined with β-cyclodextrin (β-CD) to form a KGN/β-CD inclusion complex, which was then loaded into liposomes. The KGN/β-CD-loaded liposomes were further modified with an MMP-2-responsive peptide and subsequently incorporated into a gelatin/heparin/γ-PGA (GHP) scaffold to construct an MMP-2-responsive GHP-liposome (GHP-lipo) scaffold. Finally, HB-EGF was immobilized within the GHP-lipo scaffold to prepare a GHP-HB-EGF-liposome (GHP-HB-lipo) scaffold. This scaffold promoted MSC proliferation through immobilized HB-EGF during the early stage and induced chondrogenic differentiation through MMP-2-triggered KGN release during the later stage, thereby facilitating cartilage regeneration. These scaffolds possessed multiple functions that enabled the sequential control of MSC proliferation and chondrogenic differentiation for cartilage regeneration.

## 2. Results and discussion

### 2.1 Preparation and characterization of the scaffolds

First, the GHP scaffold was fabricated using an ice particulate method.[39,40] Ice particulates with diameters ranging from 150 to 250 μm were used to control the pore sizes of the scaffolds. SEM results revealed the porous structure of the GHP scaffold, which contained large spherical pores throughout the scaffold and small pores on the walls of the larger pores, indicating that the GHP scaffold possessed a well-interconnected structure (Fig. 2a and b). Heparin staining showed a homogeneous distribution of heparin throughout the GHP scaffold (Fig. 3d). Young's modulus of the dry and hydrated scaffolds was measured using a compression test. The dry GHP scaffold exhibited a high Young's modulus (Fig. S5). After hydration, Young's modulus decreased significantly.

Meanwhile, the KGN/β-CD inclusion complex was prepared using a lyophilization method.[41,42] FT-IR spectra showed absorption peaks at 1537–1596 $cm^{-1}$, which were assigned to the C=C bonds of the aromatic ring of KGN, and absorption peaks at 1500–1600 $cm^{-1}$, which were assigned to the KGN/β-CD inclusion complex (Fig. S1). These results demonstrated the

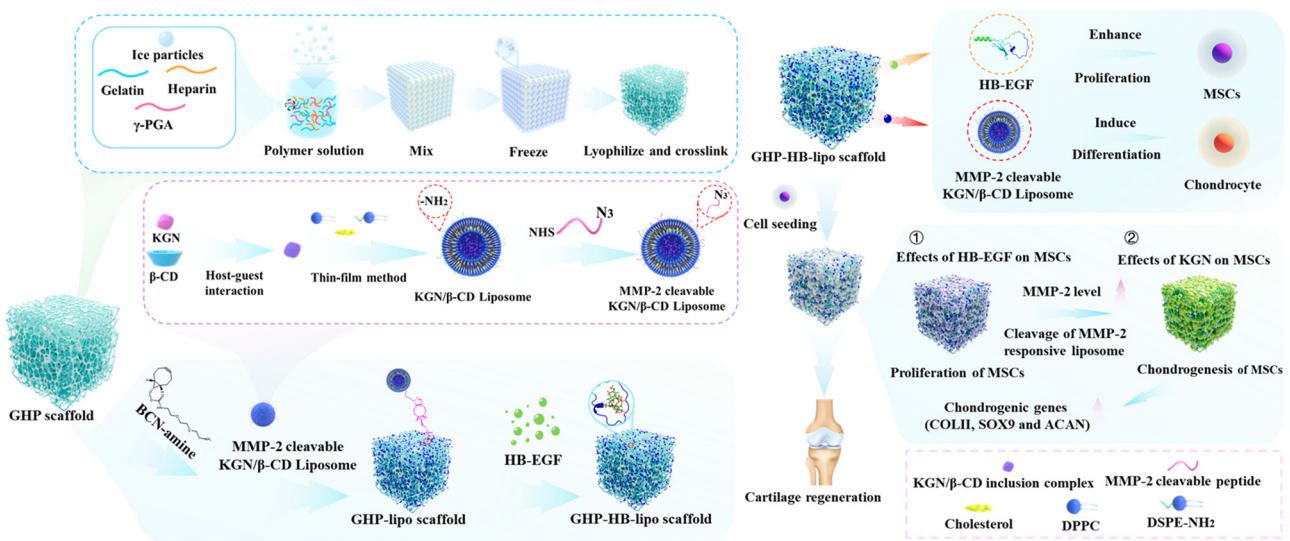



Fig. 1 Schematic illustration of the preparation of the spatiotemporally programmed GHP-HB-lipo scaffold and sequential proliferation and chondrogenic differentiation of MSCs within the scaffold for cartilage regeneration.

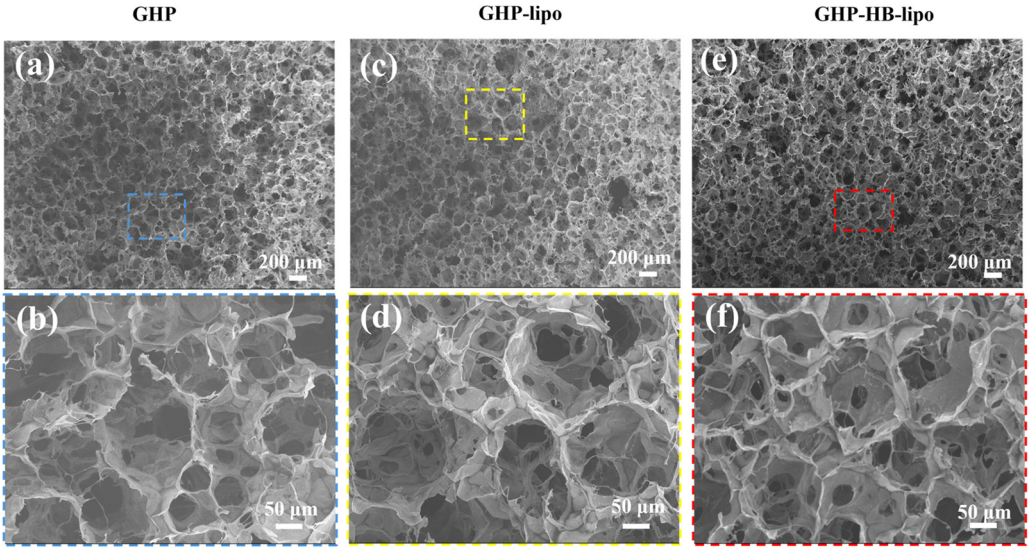



Fig. 2 Microstructures of the scaffolds: scanning electron microscopy (SEM) images of the (a) and (b) GHP scaffold, (c) and (d) GHP-lipo scaffold, and (e) and (f) GHP-HB-lipo scaffold. The images below are magnified views of the specific areas (dotted squares) shown in the images above.

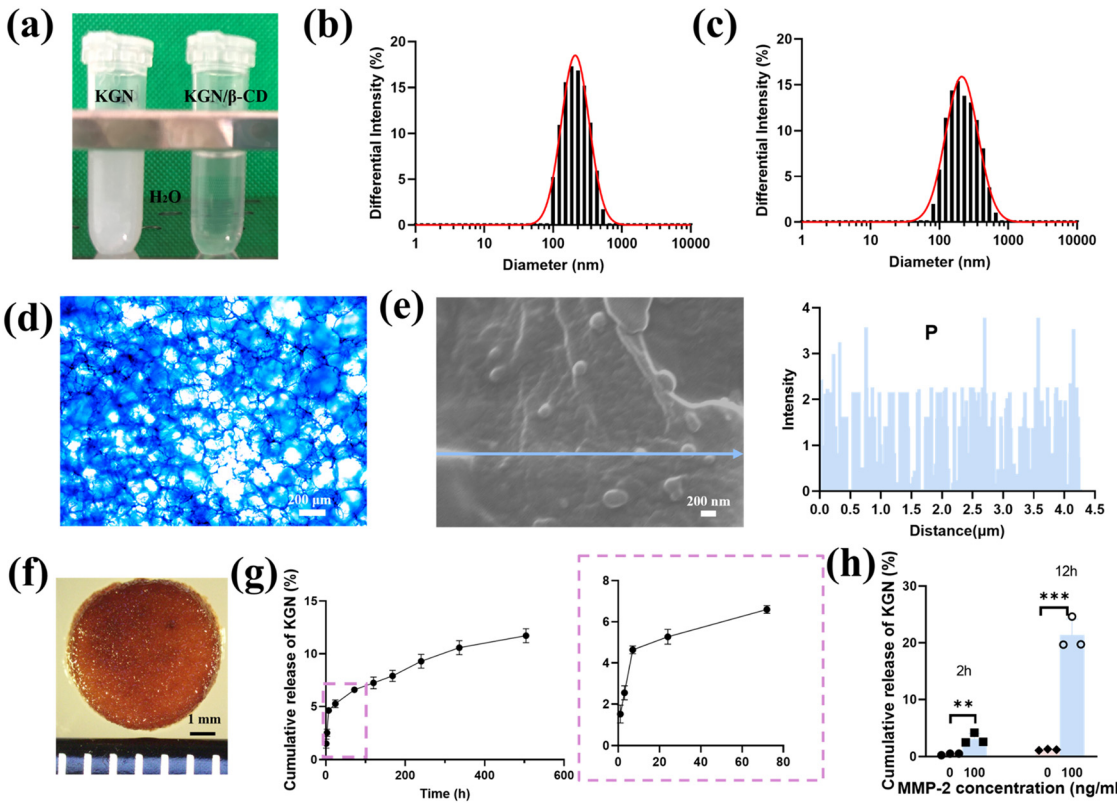



Fig. 3 Characterization of liposomes and GHP-HB-lipo scaffolds: (a) optical images of aqueous solutions of KGN and KGN/β-CD inclusion complex; hydrodynamic size distribution of (b) blank liposomes and (c) KGN/β-CD liposomes; (d) staining of heparin in GHP scaffold; (e) EDS mapping of phosphorus (P) in GHP-lipo scaffold; (f) immunochemical staining of HB-EGF in GHP-HB-lipo scaffold; (g) release profile of KGN from the GHP-HB-lipo scaffold incubated in PBS without MMP-2, where the release profile during the initial 72 h is shown in the right graph (dotted rectangle) displayed at a high magnification; and (h) release profile of KGN from GHP-HB-lipo scaffold after 2 h and 12 h of incubation in the absence or presence of MMP-2. The GHP-HB-lipo scaffold used in this experiment was pre-incubated in PBS without MMP-2 for 24 h. Data are presented as mean ± SD ($n$ = 3). Significant differences: $^{**}p < 0.01$; $^{***}p < 0.001$.

 This journal is © The Royal Society of Chemistry 2026

formation of the KGN/β-CD inclusion complex. Moreover, the UV absorption spectrum of the KGN/β-CD inclusion complex showed a strong absorption peak at approximately 276 nm, exhibiting a slight blue shift compared to that of KGN at approximately 278 nm, suggesting the successful encapsulation of KGN within the cavity of β-CD (Fig. S2). Optical images of aqueous solutions of KGN and the KGN/β-CD inclusion complex showed that the KGN/β-CD inclusion complex markedly increased the solubility of KGN (Fig. 3a). The KGN encapsulation efficiency in the KGN/β-CD inclusion complex was 88.4 ± 2.6%.

Next, the KGN/β-CD inclusion complex was encapsulated into liposomes. The encapsulation efficiency of the KGN/β-CD inclusion complex was evaluated by disrupting the KGN/β-CD liposomes and measuring the UV absorption at approximately 276 nm (Fig. S2). The encapsulation efficiency of the inclusion complex within the liposomes was 52.1 ± 3.2%. The hydrodynamic size of the KGN/β-CD liposomes was evaluated by dynamic light scattering (DLS). The KGN/β-CD liposomes and blank liposomes had mean sizes of 242.9 ± 120.4 nm and 231.4 ± 97.6 nm, respectively (Fig. 3b and c), with no significant difference between the two groups. The KGN/β-CD liposomes were further modified with an MMP-2-cleavable peptide, and the resulting MMP-2-responsive KGN/β-CD liposomes were incorporated into the GHP scaffold through click chemistry.[43]

SEM and energy-dispersive spectroscopy (EDS) mapping results confirmed the successful incorporation of MMP-2-responsive KGN/β-CD liposomes into the scaffold (Fig. 3e). The incorporation efficiency of the MMP-2-responsive KGN/β-CD liposomes was 45.1 ± 2.2%. Subsequently, HB-EGF was immobilized within the GHP-lipo scaffold to construct the GHP-HB-lipo scaffold. Immunochemical staining for HB-EGF demonstrated the successful immobilization of HB-EGF within the GHP-lipo scaffold (Fig. 3f and Fig. S3), with an immobilization efficiency of 85.2 ± 2.0%. SEM observations showed that the GHP-lipo and GHP-HB-lipo scaffolds possessed the same interconnected structure as the GHP scaffold (Fig. 2). The incorporation of MMP-2-responsive KGN/β-CD liposomes and the immobilization of HB-EGF did not affect the porous structure of the scaffolds (Fig. 2c–f).

The release profile of KGN from the GHP-HB-lipo scaffold in the absence and presence of MMP-2 was investigated (Fig. 3g and h). In PBS without MMP-2, the GHP-HB-lipo scaffold exhibited a slight initial burst release, followed by a very slow release of KGN during the 21-day incubation period (Fig. 3g). Only approximately 12% of KGN was released from the scaffold after 21 days of incubation, demonstrating the long-term stability of the KGN/β-CD inclusion complex loaded within the GHP-HB-lipo scaffold. After incubation in PBS without MMP-2 for 24 h, the GHP-HB-lipo scaffold was transferred to PBS containing MMP-2 to evaluate the MMP-2-responsive release of KGN (Fig. 3h). When incubation was continued in PBS without MMP-2, only a small amount of KGN was released. In contrast, in the presence of MMP-2, 3.1 ± 0.9% and 21.4 ± 2.8% of KGN were released from the GHP-HB-lipo scaffold after 2 h and 12 h of incubation, respectively. These results demonstrated the MMP-2-responsive release of KGN from the GHP-HB-lipo scaffold, which was attributed to the incorporation of an MMP-2-cleavable peptide serving as a linker between the KGN/β-CD liposomes and the scaffold.

### 2.2 Cell adhesion, distribution, and viability in the scaffolds

Subcultured MSCs were harvested and seeded into the scaffolds for three-dimensional (3D) culture. Cell adhesion, distribution, and viability were evaluated. As shown in Fig. 4a, the seeded MSCs adhered to the pores of the GHP-HB-lipo scaffold. MSCs in the GHP-HB-lipo scaffold exhibited adhesion behavior similar to that observed in the GHP scaffold (Fig. S4a). Nuclear staining of the vertical cross-section of the scaffold showed that MSCs were homogeneously distributed throughout the entire structure of both the GHP-HB-lipo and GHP scaffolds (Fig. 4b and Fig. S4b). Live/dead staining indicated that all cells remained viable, and no dead cells were observed in either the GHP-HB-lipo or GHP scaffold after 1 day of culture (Fig. 4c and Fig. S4c). These results indicated that both the GHP-HB-lipo and GHP scaffolds supported cell adhesion, facilitated homogeneous cell distribution, and maintained high cell viability. The incorporation of liposomes and immobilized HB-EGF did not affect cell adhesion, distribution, or viability within the scaffolds.

### 2.3 Sequential proliferation and chondrogenic differentiation of MSCs during *in vitro* culture in the GHP-HB-lipo scaffold

To investigate the effects of the GHP-HB-lipo scaffold on MSC fate regulation, the proliferation and chondrogenic differentiation of MSCs cultured in the GHP-HB-lipo scaffold were evaluated. MSCs were seeded into the GHP-HB-lipo scaffold and cultured in DMEM without the chondrogenic induction factor, KGN, for 28 days (Fig. 5a). DNA quantification showed that MSCs in the GHP-HB-lipo scaffold proliferated significantly after 7 days of culture (Fig. 5b). However, the DNA content decreased after 14 days of culture and then gradually increased again after 21 and 28 days of culture. Quantification of sGAG showed that the sGAG/DNA ratio did not change significantly after 7 days of culture but increased significantly after 14 days of culture (Fig. 5c). The sGAG/DNA ratio remained at a similar level after further culture for 21 and 28 days. Gene expression analysis showed that the expression levels of type I collagen (*COL I*), type II collagen (*COL II*), SRY-box transcription factor 9 (*SOX9*), and aggrecan (*ACAN*) did not change significantly after 7 days of culture. However, the expression levels of these genes increased significantly after 14 days of culture (Fig. 5d–g). The expression levels of *COL II*, *SOX9*, and *ACAN* continued to increase after 21 and 28 days of culture. In contrast, the expression level of *COL I* decreased after 21 and 28 days of culture. The elevated sGAG/DNA ratio and increased expression levels of *COL II*, *SOX9*, and *ACAN* demonstrated the chondrogenic differentiation of MSCs. These results indicated that MSCs cultured in the GHP-HB-lipo scaffold proliferated during the initial 7 days of culture and subsequently underwent

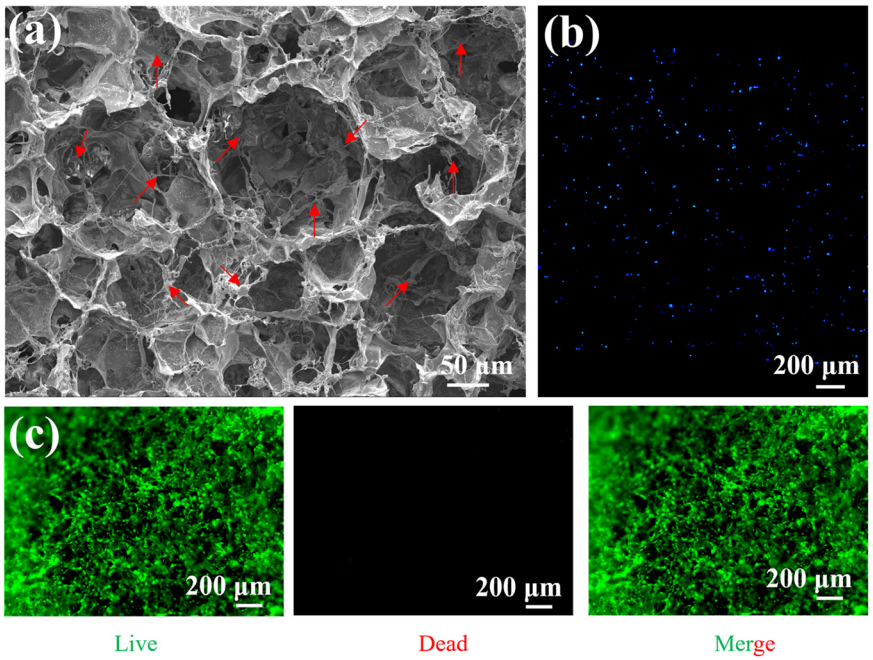



Fig. 4 Evaluation of cell adhesion, distribution, and viability after MSCs were seeded and cultured in GHP-HB-lipo scaffold for 1 day: (a) SEM image: arrows indicate MSCs; (b) nuclear staining of MSCs in the vertical cross-section of the scaffold; (c) live/dead staining of the horizontal cross-section of the scaffold. Green fluorescence indicates living cells, whereas red fluorescence indicates dead cells.

chondrogenic differentiation during the following 14, 21, and 28 days of culture.

To further demonstrate the effects of the GHP-HB-lipo scaffold on MSC proliferation and chondrogenic differentiation, the GHP-HB scaffold was used as a comparison group and seeded with MSCs in the same manner as the GHP-HB-lipo scaffold described above (Fig. 5a). MSCs seeded in the GHP-HB scaffold were cultured in KGN-free DMEM for 14 days and subsequently cultured in KGN-containing DMEM for an additional 14 days. MSCs proliferated significantly during culturing in the KGN-free medium, whereas the DNA content decreased during culturing in the KGN-containing medium (Fig. 5b). The addition of KGN to the culture medium significantly increased the sGAG/DNA ratio and the expression levels of *COL I*, *COL II*, *SOX9*, and *ACAN* (Fig. 5c–f). The immobilized HB-EGF promoted MSC proliferation, whereas the supplemented KGN in the culture medium induced chondrogenic differentiation. Compared with the GHP-HB scaffold, the GHP-HB-lipo scaffold could release KGN to induce chondrogenic differentiation without requiring additional supplementation of KGN in the culture medium.

Furthermore, immunobiological staining of chondrogenesis-related proteins (ACAN and COL II) was performed after MSCs were cultured in the GHP-HB-lipo scaffold for 7, 14, 21, and 28 days (Fig. 6b). After 7 days of culture, ACAN and COL II staining was negative. However, after 14 days of culture, weak positive staining for ACAN and COL II was observed. The staining intensity increased markedly after 21 and 28 days of culture. ACAN and COL II were not positively stained after MSCs were cultured in the GHP-HB scaffold in the KGN-free medium for 14 days. In contrast, when the cells were subsequently cultured in the KGN-containing medium for an additional 14 days, weak positive staining for ACAN and COL II was observed (Fig. 6a).

These results indicated that the GHP-HB-lipo scaffold exhibited multiple functions that promoted MSC proliferation at the early stage and induced chondrogenic differentiation at a later stage. The proliferation of MSCs during the initial 7 days of culture was likely promoted by the immobilized HB-EGF. The subsequent chondrogenic differentiation of the proliferated MSCs was likely induced by the MMP-2-triggered release of KGN. Previous studies have reported that MMP-2 expression is upregulated during MSC proliferation.[31,44,45] The upregulated MMP-2 could serve as an endogenous trigger to induce the cleavage of the MMP-2-responsive peptide, thereby releasing KGN-encapsulated liposomes from the GHP-HB-lipo scaffold (Fig. 3h). The released KGN could subsequently induce the chondrogenic differentiation of MSCs.

### 2.4. *In vivo* evaluation of the GHP-HB-lipo scaffold

To evaluate the *in vivo* efficacy of the GHP-HB-lipo scaffold, subcutaneous implantation was performed. The GHP-HB scaffold was also implanted as a comparison group. MSCs were seeded into the GHP-HB and GHP-HB-lipo scaffolds and cultured in DMEM without a chondrogenic induction factor for 12 h. The scaffolds were then subcutaneously implanted into the dorsal region of nude mice for 28 days (Fig. 7a). The implants after 28 days of implantation displayed the same round shapes as those before implantation (Fig. S6), indicating that the structure of the scaffolds was maintained during the 28 days of implantation.

DNA quantification showed that the DNA content in both the GHP-HB and GHP-HB-lipo scaffolds was significantly

 This journal is © The Royal Society of Chemistry 2026

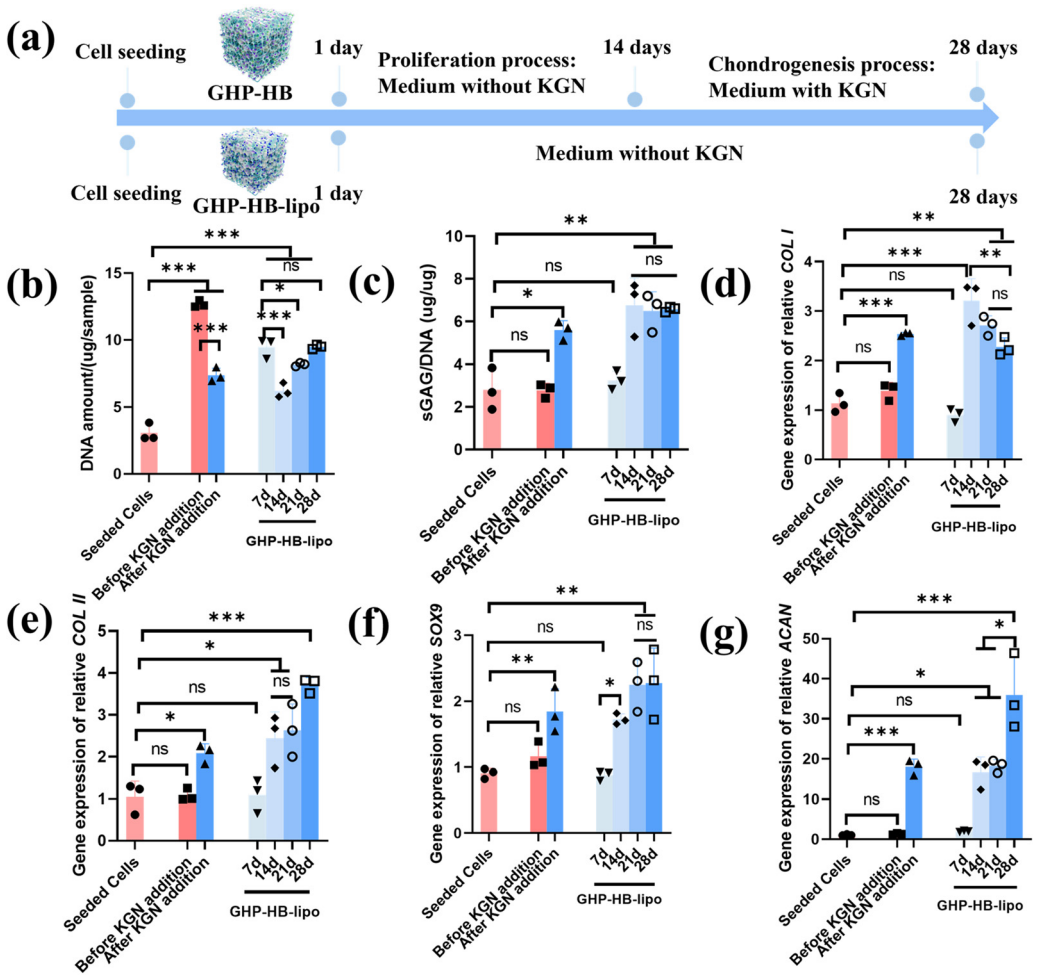



Fig. 5 Sequential proliferation and chondrogenic differentiation of MSCs in GHP-HB and GHP-HB-lipo scaffolds: (a) schematic illustration of the procedures used during 28 days of *in vitro* culture; (b) quantification of DNA content; (c) quantification of sGAG content; (d)–(g) gene expression levels of *COL I*, *COL II*, *SOX9*, and *ACAN*. The same number of MSCs used for cell seeding were used for the control. Data are presented as mean ± SD ($n$ = 3). Significant differences: *$p < 0.05$; **$p < 0.01$; ***$p < 0.001$; ns, not significant.

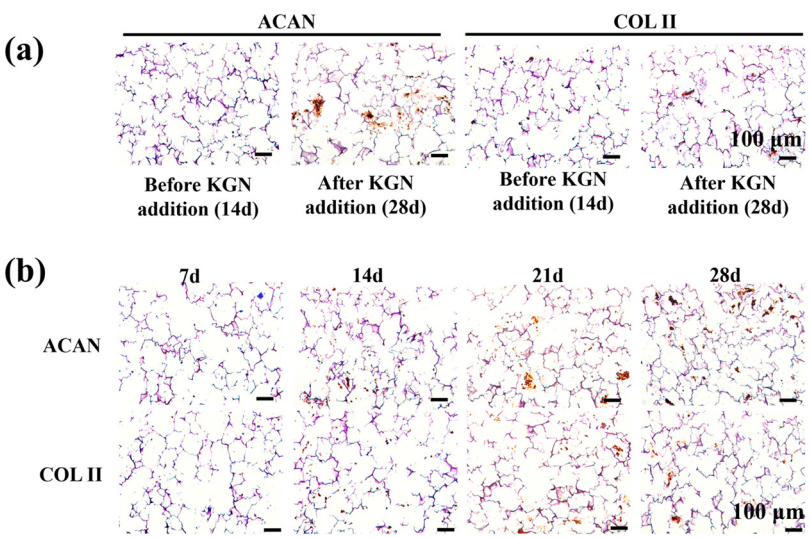



Fig. 6 Immunobiological staining of ACAN and COL II after MSCs were cultured in (a) GHP-HB scaffold after 14 day culture in absence of KGN, followed by another 14 day culture in the presence of KGN, and (b) GHP-HB-lipo scaffold for 7, 14, 21, and 28 days. Brown staining indicates positive expression of ACAN and COL II.

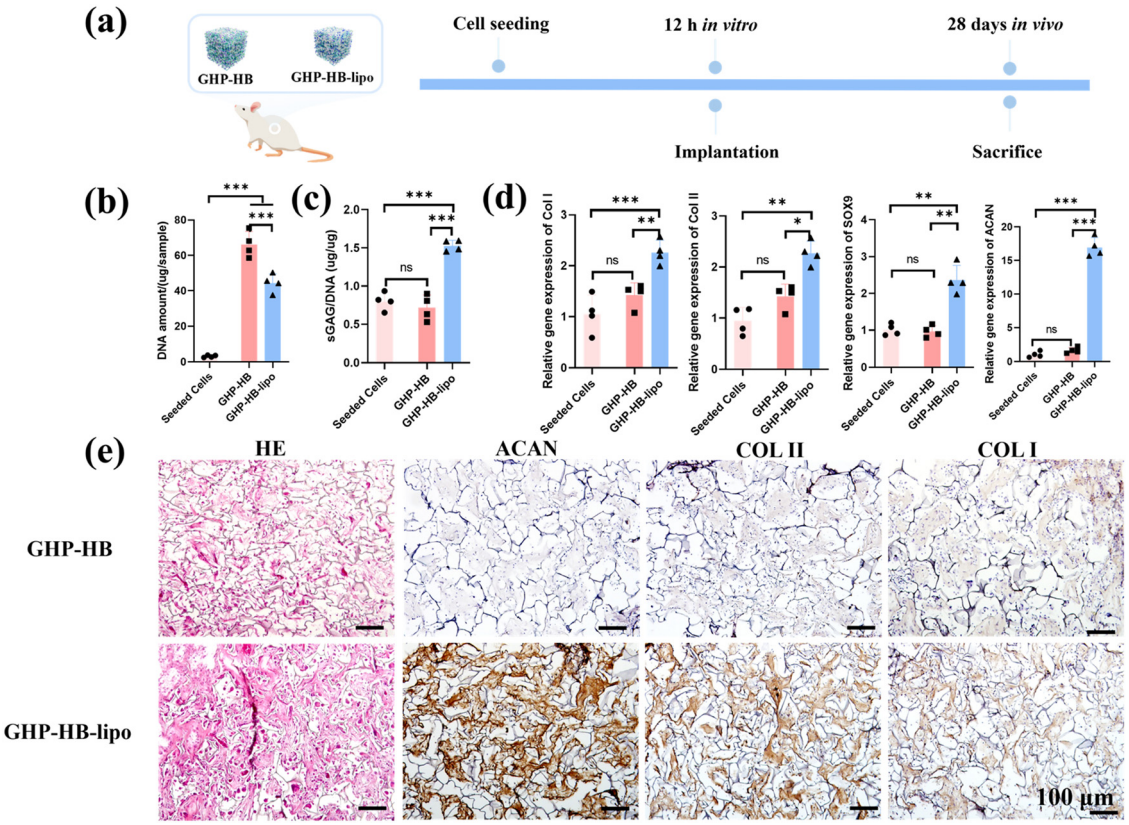



Fig. 7 *In vivo* evaluation of GHP-HB and GHP-HB-lipo scaffolds for cartilage regeneration after implantation for 28 days: (a) schematic illustration of the *in vivo* implantation procedure; (b) quantification of DNA content; (c) quantification of sGAG content; (d) gene expression levels of *COL I*, *COL II*, *SOX9*, and *ACAN*; and (e) HE staining and immunobiological staining of ACAN, COL II, and COL I. The same number of MSCs used for cell seeding were used for the control. Data are presented as mean ± SD ($n$ = 4). Significant differences: *$p < 0.05$; **$p < 0.01$; ***$p < 0.001$; ns, not significant.

higher than that of the MSCs used for seeding, indicating cell proliferation within the scaffolds (Fig. 7b). The DNA content in the GHP-HB-lipo scaffold was significantly lower than that in the GHP-HB scaffold, indicating that cell proliferation in the GHP-HB scaffold was greater than that in the GHP-HB-lipo scaffold.

Quantification of the sGAG content showed that the sGAG/DNA ratio in the GHP-HB scaffold was not significantly different from that of the MSCs used for seeding (Fig. 7c). However, the sGAG/DNA ratio in the GHP-HB-lipo scaffold was significantly higher than that in the GHP-HB scaffold. Gene expression analysis showed that the expression levels of *COL I*, *COL II*, *SOX9*, and *ACAN* in the GHP-HB-lipo scaffold were significantly higher than those in the GHP-HB scaffold (Fig. 7d). HE staining showed homogeneous cell and ECM distribution in both GHP-HB and GHP-HB-lipo scaffolds (Fig. 7e). Immunohistochemical staining indicated that ACAN and COL II were more strongly stained in the GHP-HB-lipo scaffold than in the GHP-HB scaffold. These results demonstrated that the GHP-HB-lipo scaffold was more beneficial for cartilage regeneration than the GHP-HB scaffold. This outcome was likely because the GHP-HB scaffold could only promote MSC proliferation, whereas the GHP-HB-lipo scaffold could not only enhance MSC proliferation but also promote the chondrogenic differentiation of the proliferated MSCs.

## 3. Discussion

Precise control of MSC proliferation and chondrogenic differentiation is critical for MSC-based cartilage tissue engineering. Here, we developed an artificial niche with spatiotemporal control over MSC fates by incorporating HB-EGF and KGN into a GHP scaffold. HB-EGF was immobilized through its interaction with heparin incorporated within the GHP scaffold to enhance cell proliferation, whereas KGN/β-CD liposomes were tethered through an MMP-2-cleavable peptide to induce chondrogenic differentiation. MSCs cultured in the GHP-HB-lipo scaffold exhibited initial proliferation, followed by chondrogenic differentiation. Other MMPs, such as MMP-9 and MMP-13, have also been used to achieve MMP-responsive functionality in hydrogels and scaffolds to control the release of therapeutic factors.[46,47] For example, MMP-9 has been used to control the release of anti-inflammatory and anti-rheumatic drugs to treat rheumatoid arthritis (RA) because of the elevated secretion of MMP-9 in the RA microenvironment.[46] Likewise, MMP-13 has been used to trigger the release of multiple

 This journal is © The Royal Society of Chemistry 2026

therapeutic factors in the arthritic microenvironment.[47] In this study, we used MMP-2 to trigger the release of KGN after MSC proliferation because MMP-2 has been reported to be highly expressed in proliferating stem cells and its expression increases with cell number.[30,31] The KGN/β-CD liposomes were introduced in the scaffold through tethering with an MMP-2 cleavable peptide by click chemistry.

When MSCs were cultured in the GHP-HB-lipo scaffold, the immobilized HB-EGF enhanced MSC proliferation during the initial stage without inducing chondrogenesis, which was consistent with our previous findings.[38] Following cell proliferation, MMP-2 released by the proliferated MSCs could cleave the MMP-2-cleavable peptide, thereby releasing KGN. MMP-2 secreted by MSCs is freely diffusible and can distribute throughout the culture medium. Therefore, the secreted MMP-2 should be homogenously distributed throughout the scaffold to induce chondrogenic differentiation of the proliferated MSCs. Cell culture results demonstrated the sequential proliferation and chondrogenic differentiation of MSCs during 3D culture in the GHP-HB-lipo scaffold. Animal experiments also demonstrated the sequential proliferation and chondrogenic differentiation of MSCs within the GHP-HB-lipo scaffold. These results suggested that the GHP-HB-lipo scaffold could serve as an artificial niche to direct MSC fate and holds potential for cartilage regeneration, particularly when only a limited number of donor-derived MSCs are available.

Subcutaneous ectopic implantation was used in this study. Although this model has been widely used to examine the potential of scaffolds for tissue engineering applications, it does not fully reflect the native cartilage microenvironment. Therefore, orthotopic implantation should be considered in future studies to further verify the effectiveness of the scaffold for cartilage tissue engineering.

# 4. Conclusion

In this study, we fabricated a multifunctional GHP-HB-lipo scaffold that served as an artificial niche to recapitulate the spatiotemporal control of MSC fate by immobilizing HB-EGF and MMP-2-cleavable peptide-tethered KGN-loaded liposomes within a GHP scaffold. The scaffold supported cell adhesion and promoted MSC proliferation. The KGN-loaded liposomes could be released in the presence of MMP-2, thereby inducing the chondrogenic differentiation of MSCs. *In vitro* cell culture and *in vivo* animal experiments demonstrated that the scaffold could initially promote MSC proliferation and subsequently induce the chondrogenic differentiation of the proliferated MSCs. The scaffold could serve as an artificial niche to direct MSC fate and showed promising potential for cartilage regeneration.

# 5. Experimental section

## 5.1 Preparation of the gelatin/heparin/γ-PGA (GHP) scaffold

The GHP porous scaffold was prepared using an ice particulate-based method according to our previous work, with minor modifications.[38] Briefly, ice particulates were obtained by spraying pure water into liquid nitrogen, and ice particulates with diameters of 150–250 μm were collected by sieving in a low-temperature chamber. Gelatin, heparin sodium, and γ-PGA were then dissolved separately in a 35% (v/v) acetic acid solution, and the resulting solutions were mixed to form a homogeneous solution containing 8% (m/v) gelatin, 1% (m/v) heparin sodium, and 0.2% (m/v) γ-PGA. Subsequently, the temperature of the mixed solution and the ice particulates was equilibrated at −4 °C for 6 h. The ice particulates were then added to the mixed solution at an ice-to-solution ratio of 7 : 3 (m/v), and the final mixture was transferred into a silicone mold. The construct was placed in a −80 °C freezer for 12 h. Finally, the frozen construct was lyophilized and crosslinked using a series of ethanol solutions containing EDC and NHS. After crosslinking, the scaffold was washed with Milli-Q water to obtain the GHP scaffold.

## 5.2 Microstructure characterization and heparin staining

The microstructure of the scaffold was evaluated by scanning electron microscopy (SEM; JSM-IT800, Tokyo, Japan). The distribution of heparin within the scaffold was examined by staining according to our previous work.[38] Briefly, the GHP scaffold was stained with Alcian Blue 8GX (0.5%, w/v) in 3% acetic acid for 30 min and washed three times with Milli-Q water. The stained samples were then lyophilized and examined using an optical microscope.

## 5.3 Characterization of the mechanical properties of the scaffolds

The mechanical properties of the scaffolds were evaluated by measuring their Young's modulus. The scaffolds were punched into cylindrical specimens ($\varphi$ 6 × 6 mm). Young's modulus was measured under both dry and hydrated conditions. The hydrated scaffolds were prepared by immersing the scaffolds in PBS for 2 h at room temperature. The samples were compressed at a rate of 0.1 mm $s^{-1}$ using a texture analyzer (TA-XTPlus; Texture Technologies, Hamilton, MA, USA). The initial linear region of the stress–strain curves was used to calculate Young's modulus, and three samples from each group were evaluated.

## 5.4 Preparation of the KGN/β-CD inclusion complex

The KGN/β-CD inclusion complex was prepared according to previous studies.[41,42] Briefly, 1 mM β-CD solution and 1 mM KGN solution were mixed in water and stirred at 500 rpm for 24 h in the dark at 4 °C. The solution was then filtered through a 0.45 μm filter, and the transparent filtrate was collected and lyophilized to obtain the KGN/β-CD inclusion complex. The lyophilized powder was stored in the dark at 4 °C until further use. The filter residue was collected and dissolved in DMSO, and the absorbance at 278 nm was measured by UV-vis spectrometry to calculate the encapsulation efficiency.

### 5.5 Preparation of KGN/β-CD liposomes and modification with the MMP-2-responsive peptide

1,2-Dipalmitoyl-*sn-glycero*-3-phosphocholine (DPPC), 1,2-distearoyl-*sn-glycero*-3-phosphoethanolamine-*N*-[amino-(polyethylene glycol)-2000] (ammonium salt) (DSPE–$NH_2$), and cholesterol (Chol) were used to prepare KGN/β-CD-encapsulated DPPC/Chol/DSPE liposomes (KGN/β-CD-lipo) using a thin-film hydration method. Briefly, 600 μL of DPPC (5 mg $mL^{-1}$), 320 μL of DSPE–$NH_2$ (5 mg $mL^{-1}$), and 80 μL of cholesterol (5 mg $mL^{-1}$) (molar ratio of DPPC : DSPE–$NH_2$ : Chol = 7 : 1 : 2) were mixed in a chloroform/methanol solvent mixture, and the solvent was removed by rotary evaporation under reduced pressure to form a thin lipid film. Subsequently, 1 mL of KGN/β-CD solution in PBS (1 mg $mL^{-1}$) was added to the flask for hydration, and the flask was sonicated at 45 °C for 30 min. After sonication, the suspension was extruded at 45 °C through a polycarbonate membrane with a pore size of 200 nm. The extruded suspension was centrifuged at 20 000 rpm for 15 min. The resulting sediment was washed, resuspended in 1 mL of PBS, and stored at 4 °C until further use. Dynamic light scattering (DLS; Beckman Coulter) was used to characterize the hydrodynamic size of the liposomes before and after KGN/β-CD loading. The amount of KGN/β-CD encapsulated within the liposomes was determined by disrupting the liposomes with a chloroform/methanol solvent mixture and measuring the absorbance at 276 nm using UV-vis spectrometry. The encapsulation efficiency was calculated by dividing the encapsulated amount of KGN/β-CD by the initial loading amount.

MMP-2-cleavable peptide-modified KGN/β-CD liposomes were prepared by conjugating the MMP-2-cleavable peptide to the KGN/β-CD liposomes. The peptide sequence was $N_3$-GGPVGLIGGG-CO-NHS. Briefly, 15.6 μg of the peptide was added to 1 mL of KGN/β-CD liposome suspension (KGN, 10 μM) and allowed to react at 4 °C for 6 h. The reaction mixture was then centrifuged at 20 000 rpm for 15 min to obtain the MMP-2-cleavable peptide-modified KGN/β-CD liposomes. The prepared liposomes were further washed, resuspended in PBS, and stored at 4 °C for further use.

### 5.6 Preparation of the GHP-HB-lipo scaffold

The GHP scaffold was punched into cylindrical discs ($\varphi$ 6 × 2 mm), and the discs were immersed in an EDC/NHS solution at room temperature overnight to activate the carboxyl groups. Subsequently, 57 μL of *N*-(1*R*,8*S*,9S)-bicyclo[6.1.0]non-4-yn-9-ylmethyloxycarbonyl-1,8-diamino-3,6-dioxaoctane (BCN–$NH_2$; 10.23 mg $mL^{-1}$) solution was added to the discs and allowed to react at room temperature for 12 h. Unbound BCN–$NH_2$ was removed by washing with PBS. Subsequently, 57 μL of MMP-2-responsive KGN/β-CD-lipo solution (KGN, 0.1 mg) was added to the discs and allowed to react at 4 °C for 12 h with shaking. The resulting GHP-lipo scaffold was washed with PBS, and the incorporation efficiency of the MMP-2-responsive KGN/β-CD-lipo was evaluated by immersing the GHP-lipo scaffolds in a chloroform/methanol solvent mixture and measuring the absorbance at 276 nm using UV-vis spectrometry. The incorporation efficiency was calculated by dividing the incorporated amount of MMP-2-responsive KGN/β-CD-lipo by the initial loading amount. Subsequently, the scaffold was immersed in 1 mL of HB-EGF solution (100 ng $mL^{-1}$) under shaking at 4 °C for 24 h to prepare the GHP-HB-lipo scaffold. The prepared GHP-HB-lipo scaffold was washed with PBS and stored at 4 °C for further use. The residual HB-EGF solution and PBS eluates were collected to evaluate the loading efficiency. The GHP-HB scaffold was prepared by directly immersing the GHP scaffold in 1 mL of HB-EGF solution (90 ng $mL^{-1}$) using the same procedure described above.

### 5.7 Immunochemical staining of HB-EGF

The GHP-HB-lipo scaffold was incubated overnight in PBS containing 2% bovine serum albumin at 4 °C to block non-specific antigen binding. Subsequently, the scaffold was incubated overnight at 4 °C with an anti-HB-EGF primary antibody (human HB-EGF antibody, AF-259-NA, Bio-Techne R&D Systems). After washing three times with PBS, the sample was incubated with Donkey Anti-Goat IgG H&L (Abcam) at room temperature for 2 h, followed by three washes with PBS. Color development was performed using 3,3′-diaminobenzidine (DAB) for 5 min. The stained sample was washed three times with Milli-Q water and examined by optical microscopy.

### 5.8 Immobilization efficiency of HB-EGF

The HB-EGF immobilization efficiency in the GHP-HB-lipo scaffold was measured using an enzyme-linked immunosorbent assay (ELISA) kit (human HB-EGF quantikine ELISA kit, Bio-Techne R&D Systems). The immobilized amount of HB-EGF in the scaffold was calculated by subtracting the residual amount of HB-EGF from the initial loading amount. The immobilization efficiency was calculated by dividing the immobilized amount of HB-EGF in the scaffold by the initial loading amount. Three independent samples were analyzed to calculate the mean and standard deviation.

### 5.9 KGN release from GHP-HB-lipo scaffolds

The GHP-HB-lipo scaffolds were immersed in 30 mL PBS at 37 °C with shaking. At predetermined time points, 1 mL of PBS was collected, and 1 mL of fresh PBS was added to replace the collected volume. The amount of KGN in each collected sample was measured by UV-vis spectrometry at 278 nm. The cumulative release of KGN was calculated by dividing the cumulative amount of released KGN by the initial amount of KGN in the scaffolds.

### 5.10 MMP-2-responsive release of KGN from the GHP-HB-lipo scaffold

The MMP-2-responsive release behavior of KGN/β-CD liposomes was characterized by treating the GHP-HB-lipo scaffold with MMP-2. Previous studies have reported that the upregulation of MMP-2 expression is associated with MSC proliferation.[31,44,45] The concentration of MMP-2 in the culture medium supernatant has been reported to be approximately 337.9 ng per $10^6$ cells.[48] In normal human tissues, the proportion of active MMP-2 relative

 This journal is © The Royal Society of Chemistry 2026

to total MMP-2 is approximately 20%.[49] Based on these reports and the DNA quantification results, a concentration of 100 ng $mL^{-1}$ was selected for the MMP-2-responsive release assay. The GHP-HB-lipo scaffold was equilibrated in 1 mL of PBS for 24 h and then transferred to a 24-well plate containing 1 mL of MMP-2 solution (100 ng $mL^{-1}$) and incubated with shaking at 37 °C. After 2 h and 12 h of incubation, the GHP-HB-lipo scaffold was removed, and methanol was added to each well. The absorbance of the resulting solution at 276 nm was then measured using UV-vis spectrometry. The release efficiency was calculated by dividing the released amount of KGN by the initial amount of KGN in the scaffold.

### 5.11 Culture of MSCs in the GHP-HB-lipo scaffold

Human bone marrow-derived MSCs at passage 2, obtained from Lonza (Walkersville, MD, USA), were subcultured in MSCGM™ medium. MSCs after two additional passages were collected by trypsinization and resuspended in culture medium at a concentration of $5 \times 10^6$ cells $mL^{-1}$. 57 μL of cell suspension was added to the upper surface of each GHP-HB-lipo scaffold disc and cultured for 6 h. After 6 h of culture, the scaffold discs were inverted, and the opposite side was seeded with an additional 57 μL of cell suspension. After a further 6 h, the samples were transferred to flasks containing DMEM supplemented with 2.5% FBS, 4 mM L-glutamine, and 100 U $mL^{-1}$ penicillin–streptomycin and cultured under shaking at 60 rpm. The culture was maintained for 28 days, and the medium was changed every 3 days.

### 5.12 Culture of MSCs in the GHP-HB scaffold

MSCs were seeded into GHP-HB scaffold discs using the same procedure as that described for the GHP-HB-lipo scaffold discs. MSCs in the GHP-HB scaffold were cultured in DMEM supplemented with 2.5% FBS, 4 mM L-glutamine, and 100 U $mL^{-1}$ penicillin–streptomycin under shaking at 60 rpm for 14 days. Subsequently, the culture medium was replaced with DMEM supplemented with KGN/β-CD, and the culture was continued for an additional 14 days. The medium was changed every 3 days.

### 5.13 Evaluations of cell adhesion, distribution, and viability

After MSCs were cultured in the scaffolds for 1 day, nuclear staining was performed to examine cell distribution, and live/dead staining was performed to evaluate cell viability. Cell adhesion was observed by SEM. The cell-seeded scaffolds were washed with PBS and fixed with 2.5% glutaraldehyde for 1 h. After fixation, the scaffolds were washed with Milli-Q water and lyophilized. The lyophilized scaffolds were coated with platinum and examined by SEM.

### 5.14 Quantification of DNA and sulfated glycosaminoglycan (sGAG)

MSC proliferation in the scaffolds was evaluated by quantifying DNA content. The cell/scaffold constructs were harvested at predetermined time points for quantification of the DNA and sGAG content. The harvested samples were washed, freeze-dried, and digested with papain solution at 60 °C under shaking for 12 h. The papain solution was prepared by dissolving papain in 0.1 M PBS buffer (400 μg $mL^{-1}$) containing L-cysteine hydrochloride monohydrate (5 mM) and EDTA (5 mM) at pH 6. The amounts of DNA and sGAG in the digestion solution were quantified using Hoechst 33258 and a Blyscan™ Glycosaminoglycan Assay Kit, respectively. The same number of MSCs used for cell seeding were used for the control. Three independent samples were analyzed to calculate the mean and standard deviation.

### 5.15 Real-time PCR

Samples were collected at predetermined time points for gene expression analysis. The samples were washed three times with PBS and frozen in liquid nitrogen. The frozen samples were pulverized using a crusher and lysed with 1 mL of Sepasol-RNA I Super G solution. Total RNA was extracted according to a previously reported protocol.[3] Following reverse transcription using a High-Capacity cDNA Reverse Transcription Kit, the expression of glyceraldehyde-3-phosphate dehydrogenase (GAPDH; housekeeping gene), COL I, COL II, ACAN, and SOX9 was analyzed using a QuantStudio® 3 Real-Time PCR System (Thermo Fisher Scientific). The primer and probe sequences as shown below were used. GAPDH: (forward) 5′-ATGGGGAAGGTGAAGGTCG-3′, (reverse) 5′-TAAAAGCAGCCCTGGTGACC-3′, (probe) 5′-CGCC CAATACGACCAAATCCGTTGAC-3′; COL I: (forward) 5′-CAGCCG CTTCACCTACAGC-3′, (reverse): 5′-TTTTGTATTCAATCACTGTC TTGCC-3′, (probe): 5′−CCGGTGTGACTCGTGCAGCCATC-3′; COL II: (forward) 5′GGCAATAGCAGGTTCACGTACA-3′, (reverse) 5′-CGATAACAGTCTTGCCCCACTT-3′, (probe) 5′−CCGGTATGTTT CGTGCAGCCATCCT-3′; ACAN: (forward) 5′-TCGAGGACA GCGAGGCC-3′, (reverse) 5′-TCGAGGGTGTAGCGTGTAGAGA-3′, (probe) 5′-ATGGAACACGATGCCTTTCACCACGA-3′; SOX9: (forward) 5′-CACACAGCTCACTCGACCTTG-3′, (reverse) 5′-TTCG GTTATTTTTAGGATCATCTCG-3′, (probe) 5′-CCCACGAAGG GCGACGATGG-3′. The $2^{-\Delta\Delta Ct}$ method was used to calculate the relative expression of each gene using GAPDH as the endogenous control. MSCs used for cell seeding were used as the control. The expression level of each gene was normalized to that of the control. Three independent samples were analyzed to calculate the mean and standard deviation.

### 5.16 Immunochemical staining

After MSCs were cultured in the GHP-HB-lipo scaffold for 7, 14, 21, and 28 days, the samples were collected for immunochemical staining of ACAN and COL II. The samples were washed three times with PBS and fixed with 4% paraformaldehyde for 24 h at room temperature. The fixed samples were dehydrated, embedded in paraffin, and sectioned using a microtome to obtain cross-sections with a thickness of 7 μm. The paraffin sections were deparaffinized and treated with proteinase K for 10 min for antigen retrieval, followed by blocking with a peroxidase-blocking solution for 5 min and incubation in 10% goat serum for 30 min. The sections were incubated with rabbit polyclonal anti-aggrecan antibody (1 : 100; PA1-1746, Thermo Scientific, USA) and rabbit polyclonal anti-collagen

type II antibody (1 : 100; AB746, Merck Millipore, USA) at room temperature for 2 h. After washing three times with PBS, the sections were incubated with a peroxidase-labeled polymer-conjugated secondary antibody (EnVision+ System-HRP, Dako, Japan) at room temperature for 30 min, followed by color development using 3,3′-diaminobenzidine (DAB; Dako, Japan) for 5 min. All procedures were performed at room temperature. The stained sections were examined by optical microscopy.

### 5.17 *In vivo* animal experiment

All *in vivo* experiments were conducted with approval from the Animal Experiment Ethics Committee of NIMS (accreditation no. 76-2023-10) and in accordance with the committee guidelines. GHP-HB and GHP-HB-lipo scaffold discs ($\varphi$ 6 × 2 mm) were seeded with MSCs and cultured *in vitro* for 12 h before implantation. Nude mice obtained from Charles River Laboratories (Yokohama, Japan) were used for subcutaneous implantation. After 28 days of implantation, the mice were euthanized, and the samples were collected. Quantification of the DNA content and sGAG, as well as real-time PCR analysis were conducted using the same methods described above. Four independent samples were analyzed to calculate the mean and standard deviation.

The collected samples were also used for hematoxylin and eosin (HE) staining and immunochemical staining. Paraffin sections of each sample were prepared using the same procedure described above. The paraffin sections were deparaffinized and stained with HE. Immunochemical staining of ACAN, COL II, and COL I was performed as described above using rabbit polyclonal anti-aggrecan antibody, rabbit polyclonal anti-collagen type II antibody, and rabbit polyclonal anti-collagen type I antibody (1 : 100; PA1-26204, Thermo Scientific, USA).

### 5.18 Statistical analysis

Quantitative data from multiple groups were statistically analyzed using one-way analysis of variance followed by Tukey's *post hoc* test in GraphPad Prism software (GraphPad Software, Boston, MA, USA; https://www.graphpad.com). Two-tailed *t*-tests were used to determine the significance of differences between two groups. The data are presented as the mean ± standard deviation (SD), and statistical significance is indicated as *($p < 0.05$), **($p < 0.01$), ***($p < 0.001$), and ns (not significant).

## Conflicts of interest

There are no conflicts to declare.

## Data availability

The data that support the findings of this study are available from the corresponding author upon reasonable request. Supplementary information (SI) includes the experimental data, such as FTIR and UV-vis spectra of KGN/β-CD inclusion complex; immunochemical staining of HB-EGF in GHP-lipo scaffold; mechanical properties of GHP scaffolds; cell adhesion, cell distribution and cytocompatibility of GHP scaffold, and the gross appearance of the explanted scaffolds following *in vivo* implantation. See DOI: https://doi.org/10.1039/d6tb00939e.

## Acknowledgements

This work was supported by JSPS KAKENHI Grant Number 24K03289 and JST SPRING Grant Number JPMJSP2124.

## References

1 *Articular Cartilage of the Knee: Health, Disease and Therapy*, ed. H. K. Gahunia, A. E. Gross, K. P. H. Pritzker, P. S. Babyn and L. Murnaghan, Springer New York, New York, NY, 2020.
2 C. Chung and J. A. Burdick, *Adv. Drug Delivery Rev.*, 2008, **60**, 243–262.
3 E. A. Makris, A. H. Gomoll, K. N. Malizos, J. C. Hu and K. A. Athanasiou, *Nat. Rev. Rheumatol.*, 2015, **11**, 21–34.
4 K. Johnson, S. Zhu, M. S. Tremblay, J. N. Payette, J. Wang, L. C. Bouchez, S. Meeusen, A. Althage, C. Y. Cho, X. Wu and P. G. Schultz, *Science*, 2012, **336**, 717–721.
5 T. D. Bornes, A. B. Adesida and N. M. Jomha, *Arthritis Res. Ther.*, 2014, **16**, 432.
6 U. Nöth, A. F. Steinert and R. S. Tuan, *Nat. Clin. Pract. Rheumatol.*, 2008, **4**, 371–380.
7 G. Filardo, F. Perdisa, A. Roffi, M. Marcacci and E. Kon, *J. Orthop. Surg. Res.*, 2016, **11**, 42.
8 A. Goldberg, K. Mitchell, J. Soans, L. Kim and R. Zaidi, *J. Orthop. Surg. Res.*, 2017, **12**, 39.
9 M. P. Lutolf, P. M. Gilbert and H. M. Blau, *Nature*, 2009, **462**, 433–441.
10 O. Z. Fisher, A. Khademhosseini, R. Langer and N. A. Peppas, *Acc. Chem. Res.*, 2010, **43**, 419–428.
11 C. Cha, W. B. Liechty, A. Khademhosseini and N. A. Peppas, *ACS Nano*, 2012, **6**, 9353–9358.
12 R. Schofield, *Blood Cells*, 1978, **4**, 7–25.
13 F. M. Watt and A. B. L. M. Hogan, *Science*, 2000, **287**, 1427–1430.
14 S. W. Lane, D. A. Williams and F. M. Watt, *Nat. Biotechnol.*, 2014, **32**, 795–803.
15 E. Alsberg, H. A. Von Recum and M. J. Mahoney, *Expert Opin. Biol. Ther.*, 2006, **6**, 847–866.
16 S. Tan and N. Barker, *Growth Factors*, 2013, **31**, 175–184.
17 A. K. Gaharwar, I. Singh and A. Khademhosseini, *Nat. Rev. Mater.*, 2020, **5**, 686–705.
18 B. W. H. Mui, J. J. Y. Wong, C. E. Dumas, J. H. Wang, T. Bray, K. Hirose, L. Connolly, A. Winkel, S. Timmler, N. A. Bright, E. Sliauteryte, R. T. Káradóttir, P. G. Robey, K. Franze, K. J. Chalut and M. A. Storer, *Science*, 2026, **392**, eady3136.
19 A. J. Graham, M. W. L. Khoo, V. Srivastava, S. Viragova, H. Kim, K. Parekh, K. M. Hennick, M. Bird, N. Goldhammer, J. Z. Yu, G. Hu, N. T. Brinkley, L. Pardo, J. S. Amaya, C. D. Morley, N. Chadha, P. Lebel, S. Kumar, J. M. Rosenbluth, T. J. Nowakowski, O. Chaudhuri, O. Klein,

 This journal is © The Royal Society of Chemistry 2026

R. Gómez-Sjöberg and Z. J. Gartner, *Nat. Mater.*, 2026, **25**, 1239–1251.
20 Z. Zhou, Y. Hou, Z. Yao, Q. Han, S. Wang, H. Mei, H. Chen, B. Tian, M. Li, L. Cheng, C. Zeng and Z. Dong, *Biomaterials*, 2026, **332**, 124174.
21 M. P. Lutolf and H. M. Blau, *Adv. Mater.*, 2009, **21**, 3255–3268.
22 A. J. Wagers, *Cell Stem Cell*, 2012, **10**, 362–369.
23 D. Wu, I. Eugenis, C. Hu, S. Kim, A. Kanugovi, S. Yue, J. R. Wheeler, I. Fathali, S. Feeley, J. B. Shrager, N. F. Huang and T. A. Rando, *Nat. Mater.*, 2025, **24**, 1364–1374.
24 Y. Huang, Y. Wang, G. Yang, Y. Jiang, M. Sun, S. Cheng, L. Zhong, X. Pu, B. Yang, J. Chen, Z. Chen, C. Li, L. Yang, C. Chen and J. Zhang, *Bioact. Mater.*, 2026, **57**, 660–675.
25 M. R. Hicks and A. D. Pyle, *Trends Cell Biol.*, 2023, **33**, 112–123.
26 K. S. Midwood, L. V. Williams and J. E. Schwarzbauer, *Int. J. Biochem. Cell Biol.*, 2004, **36**, 1031–1037.
27 A. E. Mayorca-Guiliani, D. J. Leeming, K. Henriksen, J. H. Mortensen, S. H. Nielsen, Q. M. Anstee, A. J. Sanyal, M. A. Karsdal and D. Schuppan, *npj Metab. Health Dis.*, 2025, **3**, 25.
28 A. Page-McCaw, A. J. Ewald and Z. Werb, *Nat. Rev. Mol. Cell Biol.*, 2007, **8**, 221–233.
29 S. G. Almalki and D. K. Agrawal, *Stem Cell Res. Ther.*, 2016, **7**, 129.
30 N. Tremain, J. Korkko, D. Ibberson, G. C. Kopen, C. DiGirolamo and D. G. Phinney, *Stem Cells*, 2001, **19**, 408–418.
31 G. Kasper, J. D. Glaeser, S. Geissler, A. Ode, J. Tuischer, G. Matziolis, C. Perka and G. N. Duda, *Stem Cells*, 2007, **25**, 1985–1994.
32 K. Johnson, S. Zhu, M. S. Tremblay, J. N. Payette, J. Wang, L. C. Bouchez, S. Meeusen, A. Althage, C. Y. Cho, X. Wu and P. G. Schultz, *Science*, 2012, **336**, 717–721.
33 N. Monteiro, A. Martins, R. L. Reis and N. M. Neves, *J. R.Soc., Interface*, 2014, **11**, 20140459.
34 S. Maritim, P. Boulas and Y. Lin, *Int. J. Pharm.*, 2021, **592**, 120051.
35 P. Bhatt, R. Lalani, I. Vhora, S. Patil, J. Amrutiya, A. Misra and R. Mashru, *Int. J. Pharm.*, 2018, **536**, 95–107.
36 L. Zhang, Q. Zhang, X. Wang, W. Zhang, C. Lin, F. Chen, X. Yang and W. Pan, *Int. J. Pharm.*, 2015, **492**, 40–45.
37 R. Gharib, H. Greige-Gerges, S. Fourmentin, C. Charcosset and L. Auezova, *Carbohydr. Polym.*, 2015, **129**, 175–186.
38 B. Peng, H. Chen, C. Lu, T. Zeng, M. Wang, T. Yoshitomi, N. Kawazoe, Y. Yang and G. Chen, *Adv. Healthcare Mater.*, 2025, e02771.
39 R. Sun, H. Chen, M. Wang, T. Yoshitomi, M. Takeguchi, N. Kawazoe, Y. Yang and G. Chen, *Biomaterials*, 2024, **307**, 122511.
40 X. Liu, H. Chen, M. Wang, T. Zeng, T. Yoshitomi, N. Kawazoe, Y. Yang and G. Chen, *Mater. Horiz.*, 2025, **12**, 8654–8666.
41 W. Wei, W. Liu, H. Kang, X. Zhang, R. Yu, J. Liu, K. Huang, Y. Zhang, M. Xie, Y. Hu and H. Dai, *Adv. Healthcare Mater.*, 2023, **12**, 2300108.
42 X. Liu, Y. Chen, A. S. Mao, C. Xuan, Z. Wang, H. Gao, G. An, Y. Zhu, X. Shi and C. Mao, *Biomaterials*, 2020, **232**, 119644.
43 R. Sun, M. Wang, T. Zeng, H. Chen, T. Yoshitomi, M. Takeguchi, N. Kawazoe, Y. Yang and G. Chen, *Bioact. Mater.*, 2025, **44**, 205–219.
44 T. Tondreau, N. Meuleman, B. Stamatopoulos, C. De Bruyn, A. Delforge, M. Dejeneffe, P. Martiat, D. Bron and L. Lagneaux, *Cytotherapy*, 2009, **11**, 559–569.
45 K. B. Fonseca, F. R. Maia, F. A. Cruz, D. Andrade, M. A. Juliano, P. L. Granja and C. C. Barrias, *Soft Matter*, 2013, **9**, 3283.
46 X. Yan, J. Zhao, M. Yan, Y. Zhu, H. Song, Y. Tian, J. Gou, H. He, T. Yin, X. Tang, X. Jiang and Y. Zhang, *J. Drug Delivery Sci. Technol.*, 2026, **115**, 107746.
47 Z. Tianyuan, D. Haoyuan, L. Jianwei, H. Songlin, L. Xu, L. Hao, Y. Zhen, D. Haotian, L. Peiqi, S. Xiang, J. Shuangpeng, G. Quanyi and L. Shuyun, *Adv. Funct. Mater.*, 2023, **33**, 2213019.
48 P. Kuchroo, V. Dave, A. Vijayan, C. Viswanathan and D. Ghosh, *Stem Cells Dev.*, 2015, **24**, 437–450.
49 Y. Weng, M. Cai, J. Zhu, J. Geng, K. Zhu, X. Jin and W. Ding, *Oncol. Res. Treat.*, 2013, **36**, 256–259.

This journal is © The Royal Society of Chemistry 2026